The Astrophysical Journal, 739:17 (5pp), 2011 September 20 doi:10.1088/0004-637X/739/1/17

INTENSITY RATIO OF DENSITY-SENSITIVE LINES IN Fe IONS OBSERVED WITH A WELL-DEFINED LABORATORY PLASMA

Nobuyuki Nakamura[1], Etsushi Watanabe[1], Hiroyuki A. Sakaue[2], Daiji Kato[2], Izumi Murakami[2], Norimasa Yamamoto[3], Hirohisa Hara[4], and Tetsuya Watanabe[4]
[1] Institute for Laser Science, The University of Electro-Communications, Chofu, Tokyo 182-8585, Japan; n_nakamu@ils.uec.ac.jp
[2] National Institute for Fusion Science, Toki, Gifu 509-5292, Japan
[3] Institute of Laser Engineering, Osaka University, Suita, Osaka 565-0871, Japan
[4] National Astronomical Observatory of Japan, Mitaka, Tokyo 181-8588, Japan
Received 2011 April 9; accepted 2011 June 30; published 2011 August 29

ABSTRACT

We present spectra of highly charged Fe ions in the extreme ultraviolet range observed using an electron beam ion trap equipped with a flat-field grazing incidence spectrometer. The density dependence of line intensity ratios is investigated for several density-sensitive lines of Fe XIII, XIV, and XV. Unlike previous studies where the electron density was estimated from theoretical considerations, here it is derived from electron beam profile measurements. The experimental data are compared with model calculations.

Key words: atomic data – atomic processes – line: formation – plasmas

Online-only material: color figures

1. INTRODUCTION

Emission lines of highly charged Fe ions in the extreme ultraviolet (EUV) range are very important for the spectroscopic diagnostics of the solar atmosphere. Important observations have been performed so far using several EUV spectrometers, such as the EUV Imaging Spectrometer (EIS; Culhane et al. 2007) on board the *Hinode* satellite, the Coronal Diagnostic Spectrometer (CDS; Harrison et al. 1995) on board the *Solar and Heliospheric Observatory* (*SOHO*) satellite, the *Solar EUV Rocket Telescope and Spectrograph* (*SERTS*; Neupert et al. 1992), and so on. For example, the EIS can observe EUV emission lines from Fe VIII to XXIV in the temperature range $4.7 \leqslant \log T_e \leqslant 7.2$. The high-quality spectra of the EIS have been providing us with opportunities to access previously unexplored fields of interest.

Recently, density diagnostics using EUV emission lines of Fe XIII have been discussed in detail. Yamamoto et al. (2008) calculated the density dependence of the line intensity ratios and compared the results with the experimental data obtained with two laboratory plasmas, an electron beam ion trap (EBIT) in Livermore and the Large Helical Device (LHD) at the National Institute for Fusion Science (NIFS) in Japan. Although good agreement between the experiments and the calculations was found, the detailed behavior of the density dependence could not be tested because only one data point from each plasma was available. The model calculations have also been compared with the EIS observation by Watanabe et al. (2009). The diagnostic capability of the Fe XIII lines was confirmed through the comparison but several problems in the atomic models were pointed out. It is thus obvious that the model should be further tested by experimental data obtained with well-defined laboratory plasmas.

An EBIT (Marrs et al. 1988) is one of the best devices for obtaining such experimental data. It consists of a Penning-like ion trap and an electron beam going through the trap. Highly charged ions are produced through the successive ionization events caused by the beam electrons, and trapped for hours while interacting with the high-energy electrons. The plasma in an EBIT is a simple non-neutral plasma composed of trapped ions and a quasi-monoenergetic electron beam. The emission spectra obtained with an EBIT can thus provide a high-quality benchmark for testing model calculations.

Liang et al. (2009a, 2009b) have used the FLASH-EBIT (Epp et al. 2007) in Heidelberg to investigate density-sensitive lines of highly charged Fe ions in the EUV range 100–350 Å. Line intensity ratios were obtained for density-sensitive lines of Fe X, XI, XII, XIII, XIV, XXI, and XXII with several electron beam parameters and compared with model calculations. They found discrepancies between the experiment and the model when the electron density was estimated from the theoretical electron beam width (Herrmann 1958), and concluded that the discrepancies arose from the incomplete overlap between the electron beam and the trapped ion cloud.

In this paper, we present EUV spectra obtained with a compact low-energy EBIT (Nakamura et al. 2008) recently developed in Tokyo. The main objective of this study is to obtain the intensity ratios of density-sensitive lines under well-defined conditions so that the data can act as a benchmark for density-dependent models. The density of the beam electrons has thus been experimentally determined by measuring the profile of the electron beam. In addition, the spatial distribution of the trapped ions has been observed so that the overlap effect can be examined. The experimental results obtained for Fe XIII, XIV, and XV are compared with model calculations.

2. EXPERIMENT

Figure 1 shows the experimental setup used in the present study. In this experiment, a compact EBIT developed at the University of Electro-Communications, called CoBIT, was used. Details of the CoBIT device have been described in previous papers (Nakamura et al. 2008; Sakaue et al. 2010). Briefly, the device mainly consists of an electron gun, an ion trap, and an electron collector. The ion trap consists of three successive drift tubes and a superconducting magnet surrounding them. The drift tubes provide a well potential which traps the ions axially, and the axial magnetic field produced by the superconducting magnet can trap the ions radially. The magnetic field is also used

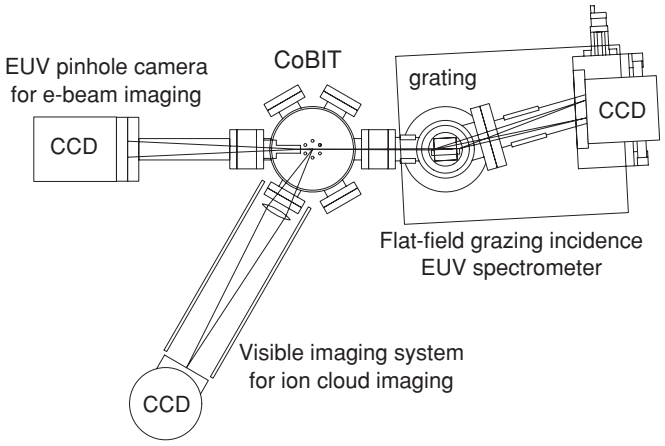

Figure 1. Schematic drawing of the experimental setup.

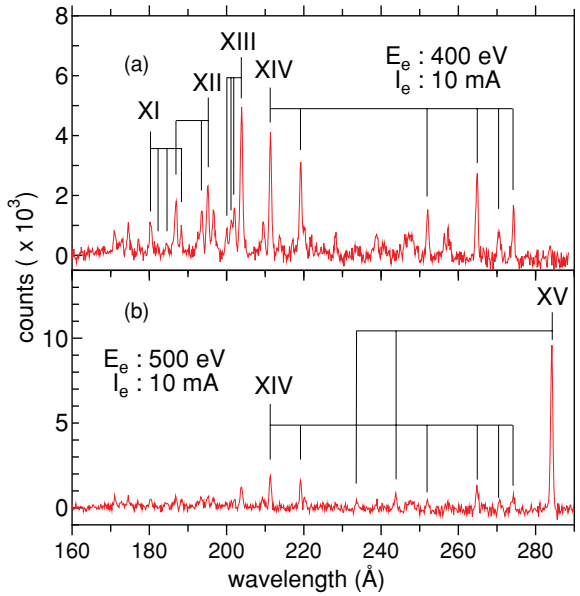

Figure 2. Typical spectra obtained with CoBIT. E_e and I_e denote the electron beam energy and current at which the spectrum was obtained.

(A color version of this figure is available in the online journal.)

to compress the electron beam going through the trap. The space charge potential of the compressed beam electrons can also help to trap ions radially. Highly charged ions are produced through successive electron impact ionization and trapped in the middle of the drift tube.

In the present experiment, Fe ions were produced by introducing $Fe(C_5H_5)_2$ vapor into CoBIT through a variable leak valve. The ions produced were trapped with a trapping potential of 30 V applied to the both ends of the drift tubes. EUV emission from the trapped ions excited by the beam electrons was observed with a grazing incidence flat-field grating spectrometer (Sakaue et al. 2009). This consisted of a laminar-type diffraction grating with a groove number of 1200 gr mm^{-1} (Shimadzu 30-002) and a Peltier-cooled back-illuminated CCD (Roper PIXIS-XO: 400B). In the present setup, no entrance slit was used because the EBIT represents a line source which can be regarded as a slit. The spectral resolution of the present arrangement was typically 0.8 Å, which was mainly limited by the electron beam width.

Typical spectra obtained at electron energies of 400 and 500 eV are shown in Figure 2, and the lines of present interest are listed in Table 1. The spectra indicate that the plasma in CoBIT

Table 1
Lines of Present Interest

Ion	Lower Level	Upper Level	Wavelength (Å)
Fe XIII	$3s^23p^2\ ^3P_1$	$3s^23p3d\ ^3D_2$	200.022
	$3s^23p^2\ ^3P_0$	$3s^23p3d\ ^3P_1$	202.044
	$3s^23p^2\ ^3P_1$	$3s^23p3d\ ^3P_0$	203.164
	$3s^23p^2\ ^3P_2$	$3s^23p3d\ ^3D_2$	203.797
	$3s^23p^2\ ^3P_2$	$3s^23p3d\ ^3D_3$	203.828
	$3s^23p^2\ ^3P_1$	$3s^23p3d\ ^1D_2$	204.263
Fe XIV	$3s^23p\ ^2P_{1/2}$	$3s^23d\ ^2D_{3/2}$	211.318
	$3s^23p\ ^2P_{3/2}$	$3s^23d\ ^2D_{5/2}$	219.131
	$3s^23p\ ^2P_{3/2}$	$3s3p^2\ ^2P_{3/2}$	264.790
	$3s^23p\ ^2P_{3/2}$	$3s3p^2\ ^2P_{1/2}$	270.522
	$3s^23p\ ^2P_{1/2}$	$3s3p^2\ ^2S_{1/2}$	274.204
Fe XV	$3s3p\ ^3P_2$	$3s3d\ ^3D_3$	233.866
	$3s3p\ ^1P_1$	$3s3d\ ^1D_2$	243.794

Note. The wavelength values are taken from the CHIANTI database.

had a narrow charge state distribution. For example, emission lines from Fe XII to XIV were predominantly observed with an electron energy of 400 eV. When the energy was increased to 500 eV, however, the abundance of Fe XII and XIII became very small and emission lines from Fe XIV and Fe XV were predominantly observed. This narrow charge distribution is important for obtaining clean spectra with less line overlap. Since the observations were performed only at 90° with respect to the electron beam, polarization could affect the line intensity. Liang et al. (2009a) estimated the polarization effect on the line intensity ratio and confirmed that the effect is less than 10% for almost all transitions in Fe XIII and XIV. We have estimated the effect for Fe XV and confirmed that it is also less than 10%. Thus the polarization effect is not considered.

At the same time as the spectral observation, the electron beam profile was measured with a pinhole camera to obtain the density of the beam electrons. A slit, 0.2 mm wide, was placed 30 mm from the electron beam and the EUV photons passing through the slit were observed with another Peltier-cooled back-illuminated CCD placed 320 mm from the slit. This arrangement enabled us to obtain the spatial distribution of the EUV emission with a magnification of about 10. The EUV emission distribution is considered to represent the electron density distribution since the lifetime of EUV transitions is as short as the order of 10^{-10} s. The distribution was a nearly Gaussian shape with a typical width (full width at half-maximum) of about 0.4 mm (Sakaue et al. 2010), which gave an average density of the order of 10^9–10^{10} cm^{-3} for the electron energy and current ranges studied. Although the CCD is also sensitive to visible transitions with a long lifetime, we confirmed that the contribution from visible light was negligibly small by observation through an optically transparent glass.

In an EBIT, trapped ions can range over an area that is wider than that covered by the beam electrons (Liang et al. 2009b). If the overlap factor between the electron beam and the ion cloud is not unity, the "effective" electron density which the trapped ions experience should be different from the "actual" electron density. In order to confirm the overlap between the electron beam and the ion cloud, we also measured the spatial distribution of the visible emission using a simple imaging system consisting of a biconvex lens and a liquid-nitrogen-cooled CCD. Since most visible transitions in highly charged ions are M1 transitions between fine-structure levels, the lifetime is usually as long as the order of 10^{-3} s, which is long enough compared to the motion

of the trapped ions. Thus, the spatial distribution of the visible emission is considered to represent the spatial distribution of ions.

3. THEORETICAL MODEL

In order to estimate the measured intensity ratios, a collisional-radiative model for Fe XIII–XV was constructed (Yamamoto et al. 2008). Rate equations in the model were solved to assume quasi-steady states and population densities for the fine structure of 894 ($3s^2 3pnl$, $3s3p^2nl$, $3p^3nl$) states on Si-like, 332 ($3s^2nl$, $3s3pnl$, $3s3d^2$, $3p^3$, $3p^23d$, and $3d^3$) states on Al-like, and 283 ($3snl$, $3pnl$, and $3dnl$) states on Mg-like ions up to the principal quantum number $n = 5$. Line intensities were calculated by multiplying population densities by radiative transition rates. In the model, atomic processes include excitation/de-excitation and ionization by electron impact, then radiative transition. Cross sections and transition probabilities were calculated with HULLAC (Bar-Shalom et al. 2001). The electron velocity distribution in the calculation of reaction rate is the delta function at a velocity corresponding to electron beam energy. Radiative transition rates on the $3s^2 3p^2$, $3s3p^3$, $3p^4$ states of Si-like ions adopted in the present model were calculated by the GRASP code (Keenan et al. 2007). Line wavelengths were corrected by data from CHIANTI (Dere et al. 1996; Landi et al. 2006).

4. RESULTS AND DISCUSSION

The intensity ratios obtained for several density-sensitive lines of Fe XIII–XV are plotted as a function of the electron density in Figure 3. The data obtained with electron beam energies of 400 and 500 eV are plotted as open and closed squares, respectively. The "actual" electron density determined from the electron current and the electron beam profile observed with the pinhole EUV camera was used as a horizontal axis rather than the "effective" electron density which could be obtained by taking the overlap between the electrons and ions into account. The ion distribution (visible emission distribution) measurement always gave a broader distribution compared to the electron distribution (EUV distribution), so that the "effective" electron density should be smaller than the "actual" electron density. However, since the intensity of the visible light was so weak, a clear image was not always successfully obtained. Thus, the overlap effect was estimated from typical results to be 40% at the maximum, and is reflected to the negative horizontal error bar. Our result may contradict previous observations with the FLASH-EBIT by Liang et al. (2009b), where the expansion of the ion cloud radius was estimated to be as large as about 5–10 with respect to the electron beam size. However, we must note that the EBIT operational parameters were very different from each other. For example, the electron beam width of the present measurement was larger than that in the FLASH-EBIT by a factor of more than 10 (about 0.5 mm in the present experiment and about 0.03 mm in the FLASH-EBIT experiment). Furthermore, both the electron energy and the current were much lower than those in the FLASH-EBIT. It is thus more likely that the large difference in the operational parameters resulted in the large difference in the overlap factor. The vertical error bars represent the error estimated from fitting with the Gaussian peak profiles. No sensitivity correction was made since the ratio is investigated between nearby lines for which the sensitivity of the spectrometer (including the efficiency of the CCD) is considered to be approximately the same. Solid lines in the figure represent the result of the present model calculations. In the following subsections, the result for each charge state is discussed in more detail.

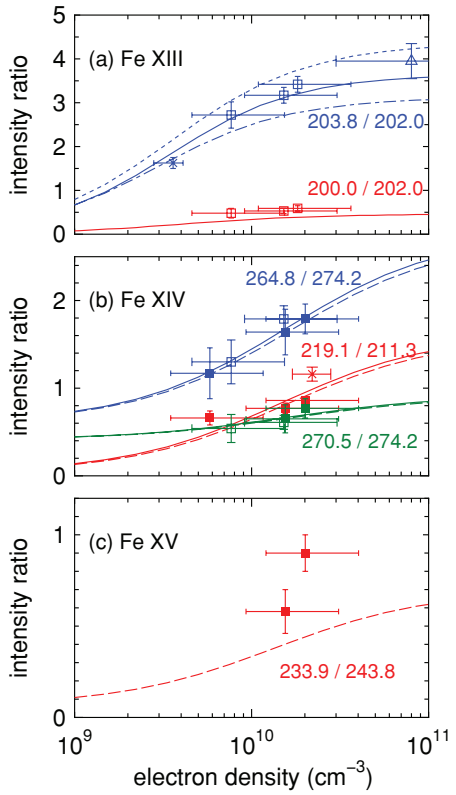

Figure 3. Intensity ratio of density-sensitive lines of (a) Fe XIII, (b) Fe XIV, and (c) Fe XV. The data obtained with electron beam energies of 400 and 500 eV are plotted as open and closed squares, respectively. The vertical error bars were estimated from fitting with the Gaussian peak profiles. The horizontal error bars have different meanings depending on their sign. The positive error bar represents the maximum assumed electron density at the center of the Gaussian electron beam. The negative error bar represents the effect of the overlap between the electron beam and the trapped ion cloud (see the text for details). Previous experimental values by Yamamoto et al. (2008) and Liang et al. (2009a) are also plotted as a triangle and crosses, respectively. The solid and long dashed lines represent the results of the present model calculation for 400 and 500 eV, respectively. See the text for the short dashed and dot-dashed lines in (a).

(A color version of this figure is available in the online journal.)

4.1. Fe XIII

As already mentioned in the introduction, the intensity ratio of the Fe XIII lines around 200 Å is one of the most important diagnostic measures for electron density in the solar corona (Yamamoto et al. 2008; Watanabe et al. 2009). Watanabe et al. (2009) discussed the density diagnostics using line intensity ratios among about 10 lines observed by EIS around 200 Å. Unfortunately, however, the spectral resolution of the present measurement was not enough to resolve all of them. The close-up spectrum at the region of interest is shown in Figure 4 together with model spectra. For example, the strongest line at 203.8 Å might be composed of four contributions: 203.16, 203.80, 203.83, and 204.26 Å. The experimental ratio 203.8/202.0 in Figure 3(a) is thus compared with two theoretical values: one is (203.80+203.83)/202.04 (solid line) and another is (203.16+203.80+203.83+204.26)/202.04 (dashed line). As shown in the figure, the experimental results fall between them. Although weak emission lines from other charge states, e.g.,

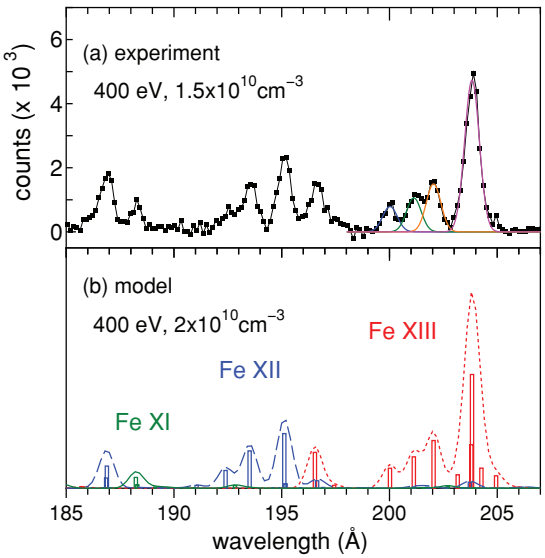

Figure 4. (a) Experimental spectrum (black) obtained with a 400 eV–10 mA electron beam. The electron density was estimated to be 1.5×10^{10} cm^{-3} from the electron beam profile measurement. The colored solid lines represent the Gaussian profiles of Fe XIII fitted to the experimental spectrum. (b) Model spectra for Fe XI (solid line), Fe XII (long dashed line), and Fe XIII (short dashed line) obtained by convoluting the theoretical intensity (white bars) with an experimental resolution. A monoenergetic electron beam of 400 eV with a density of 10^{10} cm^{-3} was assumed in the calculation. The ratio among Fe XI to Fe XIII was adjusted to fit the experimental data.

(A color version of this figure is available in the online journal.)

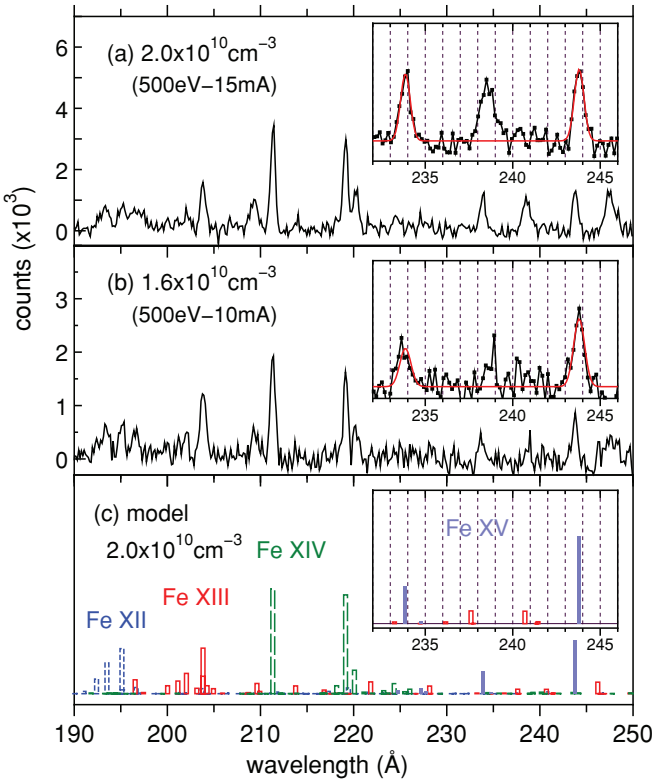

Figure 5. (a and b) Electron density dependence of the spectra obtained at an electron energy of 500 eV. Insets show the close-up for the region where Fe XV lines were observed. The red solid line in the inset represents the result of fitting performed to obtain the ratio plotted in Figure 3(c). (c) Theoretical intensity of Fe XII (blue dashed line), Fe XIII (red solid line), Fe XIV (green long dashed line), and Fe XV (purple solid bar). The ratio among the different charge states was adjusted to fit the experimental data.

(A color version of this figure is available in the online journal.)

203.73 of Fe XII and 202.71 of Fe XI could also overlap with the Fe XIII lines, we consider from the comparison with the model spectra that such contributions should be smaller than the present experimental error.

It should be noted that there exist two possible candidates for the wavelength of the $3s^2 3p^2\ ^3P_1$–$3s^2 3p 3d\ ^3P_0$ transition as pointed out by Keenan et al. (2007). One is 202.42 Å as listed in the National Institute of Standards and Technology database, and another is 203.16 Å as assigned by Landi (2002) and listed in the CHIANTI database. Keenan et al. (2007) have suggested that 203.16 is more favorable based on the intensity ratio to the 200.03 line. If it is 202.42, the line should overlap with 202.04 under the present experimental resolution; the experimental result should thus be compared with (203.80+203.83+204.26)/(202.04+202.42), which is shown by the dot-dashed line in Figure 3(a). The agreement with the (203.16+203.80+203.83+204.26)/202.04 ratio (dashed line) and the disagreement with the (203.80+203.83+204.26)/(202.04+202.42) ratio (dot-dashed line) are consistent with the suggestion by Keenan et al. (2007).

The origin of the 202.4 line has been discussed so far in several papers. Brosius et al. (1998) and Brown et al. (2008) assigned both the 203.2 and 202.4 lines to Fe XIII. However, we believe that this is unlikely because the number of the possible transitions in Fe XIII is limited, and only one line corresponding to the $3s^2 3p^2\ ^3P_1$–$3s^2 3p 3d\ ^3P_0$ transition should exist between the lines at 202.044 and 203.797 Å. Keenan et al. (2007) proposed the possibility that the line assigned as the second order of 202.44 Å in the *SERTS* observation was the first order of the Fe V $3d^4\ ^3D_2$–$3d^3 4p\ ^3D_1$ transition at 404.87 Å. The 202.4 line has, however, been observed in the first-order spectra of EIS. Landi & Young (2009) assigned the 202.42 line to Fe VII $3p^6 3d^2\ ^3F_4$–$3p^5 3d^3(^2F)^1G_4$, and more recently Del Zanna (2010) assigned it to Fe XI $3p^4\ ^3P_2$–$3p^3 3d\ ^3P_2$. In each case, it would be too weak to contribute to the present observed line at 202.0 Å, i.e., the denominator of the experimental ratio 203.8/202.0 plotted in Figure 3(a), because the charge state distribution is so narrow that the abundance of both Fe VII and Fe XI is much smaller than that of Fe XIII.

4.2. Fe XIV

As seen in Figure 2 and also in Figure 5, since the emission lines of Fe XIV are scattered over a rather wide range, it is considered that no serious line overlap exists for Fe XIV. The intensity ratios for 264.8/274.2, 219.1/211.3 and 270.5/274.2 are plotted as a function of the electron density in Figure 3(b). Again, good agreement between the experiments and the calculations is found. It seems that there exists a small deviation between the experiment and the model at the lowest density data. However, the experimental uncertainties are not small enough to discuss this deviation. As seen in the figure, it can be confirmed from both theoretical and experimental results that the energy dependence is small.

4.3. Fe XV

In the present wavelength range of interest, Fe XV represents a very strong resonance line at 284.2 Å as shown in Figure 2. However, since no other lines were observed near the strong line, we studied the ratio between 233.9 Å and 243.8 Å, which are close enough in wavelength not to be significantly affected by the responsivity function of the detector and the grating.

The results are shown in Figure 3(c). The two data points were obtained with electron currents of 10 and 15 mA. The observation was also made with a current of 5 mA, but the line intensity was too small to obtain meaningful statistics.

As seen in the figure, the experimental result seems to have a strong dependence on the density, which results in poor agreement with the model prediction. Figure 5 shows the original spectra used for obtaining the intensity ratio plotted in Figure 3(c). As confirmed in the figure, the relative intensity of 233.9 Å became very strong for higher electron current, i.e., higher electron density. A line of Fe XIII, which is close in wavelength (233.2 Å), may overlap with the 233.9 Å line. However, the 233.2 Å line could not be observed even at an electron energy of 400 eV where the abundance of Fe XIII was much higher (see Figure 2(a)). In addition, the profile of the 233.9 Å line does not seem to have any shoulder. It is thus considered that the overlap of the 233.2 Å line does not exist. Furthermore, no line is available either for possible residual gas ions such as carbon, oxygen, and so on. Consequently, we consider that future improvement of the model calculation is needed to explain the experimental result. It may be noted that the line from O IV, whose wavelength is 238.4 Å, is found to have increased as the electron current increased. The contamination often increases with the electron current probably due to outgassing from the collector or somewhere else. Actually, the amount of contamination strongly depends on the vacuum condition. To examine the influence of the contamination on the Fe XV ratio, we have observed spectra with the same electron beam condition but with different vacuum conditions. It has been confirmed that the reproducibility of the Fe XV ratio is good independent of the amount of contamination.

5. SUMMARY AND OUTLOOK

EUV spectra of highly charge Fe ions were observed using a compact EBIT with a flat-field grazing incidence spectrometer under well-defined experimental conditions. The density dependence of several density-sensitive lines in Fe XIII, XIV, and XV was compared with model calculations and overall good agreement was found. For the ratio 233.9/243.8 of Fe XV, however, we consider that improvement of the model is required.

The present experimental errors are mainly limited by the stray light background arising from the cathode of the electron gun. Compared to ordinary EBITs, the distance between the ion trap and the cathode is much smaller for the compact EBIT used in the present study; stray light thus causes serious background. Two possible solutions are considered. The first is to use a microchannel plate (MCP) as a detector of the spectrometer. Since an MCP coated with CsI has good sensitivity for EUV photons but practically no sensitivity for visible photons, clear spectra without stray light are expected to be obtained. However, one should note that the position resolution of an MCP is not good as that of a CCD, which may result in poor spectral resolution. The second is to use a filter in front of the CCD. For example, a thin aluminum filter, which has a good transmittance for EUV photons, is commercially available. Furthermore, a higher-resolution spectrometer has recently been developed. This will enable us to resolve the lines which overlapped in the present study. These improvements are in progress; we hope to report the improved results in the near future.

This work was performed under the Research Cooperation Program in the National Institutes of Natural Sciences (NINS).

REFERENCES

Bar-Shalom, A., Klapisch, M., & Oreg, J. 2001, J. Quant. Spectrosc. Radiat. Transfer, 71, 169
Brosius, J. W., Davila, J. M., & Thomas, R. J. 1998, ApJS, 119, 255
Brown, C. M., Feldman, U., Seely, J. F., Korendyke, C. M., & Hara, H. 2008, ApJS, 176, 511
Culhane, J., Harra, L. K., James, A. M., et al. 2007, Sol. Phys., 243, 19
Del Zanna, G. 2010, A&A, 514, A41
Dere, K. P., Landi, E., Mason, H. E., Fossi, B. C. M., & Young, P. R. 1996, A&AS, 125, 149
Epp, S. W., López-Urrutia, J. R. C., Brenner, G., et al. 2007, Phys. Rev. Lett., 98, 183001
Harrison, R. A., Sawyer, E. C., Carter, M. K., et al. 1995, Sol. Phys., 162, 233
Herrmann, G. 1958, J. Appl. Phys., 29, 127
Keenan, F. P., Jess, D. B., Aggarwal, K. M., et al. 2007, MNRAS, 376, 205
Landi, E. 2002, A&A, 382, 1106
Landi, E., Del Zanna, G., Young, P. R., et al. 2006, ApJS, 162, 261
Landi, E., & Young, P. R. 2009, ApJ, 706, 1
Liang, G. Y., Baumann, T. M., López-Urrutia, J. R. C., et al. 2009a, ApJ, 696, 2275
Liang, G. Y., López-Urrutia, J. R. C., Baumann, T. M., et al. 2009b, ApJ, 702, 838
Marrs, R. E., Levine, M. A., Knapp, D. A., & Henderson, J. R. 1988, Phys. Rev. Lett., 60, 1715
Nakamura, N., Kikuchi, H., Sakaue, H. A., & Watanabe, T. 2008, Rev. Sci. Instrum., 79, 063104
Neupert, W. M., Epstein, G. L., Thomas, R. J., & Thompson, W. T. 1992, Sol. Phys., 137, 87
Sakaue, H. A., Kato, D., Nakamura, N., et al. 2009, J. Phys.: Conf. Ser., 163, 012020
Sakaue, H. A., Nakamura, N., Watanabe, E., Komatsu, A., & Watanabe, T. 2010, J. Instrum., 5, C08010
Watanabe, T., Hara, H., Yamamoto, N., et al. 2009, ApJ, 692, 1294
Yamamoto, N., Kato, T., Funaba, H., et al. 2008, ApJ, 689, 646